Aperture Selection for ACO-OFDM in Free-Space Optical Turbulence Channel

Junyi Jiang, Peichang Zhang, Rong Zhang, *Member, IEEE*, Sheng Chen, *Fellow, IEEE*, and Lajos Hanzo, *Fellow, IEEE*

***Abstract*—We propose a novel aperture selection (ApS) scheme for an asymmetrically-clipped-optical-orthogonal-frequency-division-multiplexing-based (ACO-ODFM) multiple-transmit/receive-aperture (MT/RA) system communicating over a free-space optical (FSO) turbulence channel between a pair of cooperating base stations in a vehicular communication system. Our proposed ApS scheme is capable of significantly improving the system's achievable diversity gain, bit error ratio (BER), and throughput, while imposing substantially reduced power consumption and hardware complexity. Our results demonstrate that the proposed system's performance was improved more significantly under strongly turbulent channel conditions.**

***Index Terms*—Aperture selection (ApS), asymmetrically clipped optical orthogonal frequency-division multiplexing (ACO-OFDM), free-space optical (FSO) turbulence channel, multiple transmit/receive aperture (MTRA).**

I. Introduction

FREE-SPACE OPTICAL (FSO) links [1], [2] provide an attractive design alternative for base station–base station in cooperative multicell scenarios [3], [4] to the classic radio frequency (RF) microwave links, where the turbulent outdoor channel suffers from adverse propagation conditions. They also offer a design alternative for the extremely challenging aircraft-to-aircraft and aircraft-to-satellite vehicular communication scenarios [5]–[7], with the goal of providing sophisticated wireless multimedia service and Internet access above the clouds [8]. While, at the time of writing, most of the solutions considered in the literature rely on radio communications with satellites [9]–[16], we believe that an FSO solution may also be developed for this emerging vehicular communication scenario. Therefore, multiple transmit/receive aperture (MTRA)-aided techniques may be invoked, both for increasing the system's throughput and for acquiring a diversity gain [17]. Hence, MTRA techniques are capable of offering an improved bit error ratio (BER) by mitigating the aforementioned detrimental propagation effects of FSO communications at the expense of increasing hardware complexity and power consumption.

Manuscript received November 18, 2014; revised April 15, 2015 and July 14, 2015; accepted August 19, 2015. Date of publication August 21, 2015; date of current version August 11, 2016. This work was supported by Research Councils UK under the auspices of the India–U.K. Advanced Technology Center and of the European Union CONCERTO Project, as well as the European Research Council's Advanced Fellow Grant. The review of this paper was coordinated by Prof. Y. Gong.

The authors are with the Department of Electronics and Computer Science, University of Southampton, Southampton SO17 1BJ, U.K. (e-mail: jj4e09@ecs.soton.ac.uk; pz3g09@ecs.soton.ac.uk; rz@ecs.soton.ac.uk; sqc@ecs.soton.ac.uk; lh@ecs.soton.ac.uk).

Color versions of one or more of the figures in this paper are available online at http://ieeexplore.ieee.org.

Digital Object Identifier 10.1109/TVT.2015.2471809

Asymmetrically clipped optical orthogonal frequency-division multiplexing (ACO-OFDM) has been used in numerous systems designed for indoor visible light communication [18]–[20], despite its factor 4 throughput reduction imposed by its Hermitian symmetry, which has to be satisfied for the sake of generating real and positive-valued optical modulated signals. Although the indoor propagation of light only imposes mild dispersion in moderately sized rooms, ACO-OFDM has the innate ability to eliminate the dispersion imposed by multipath reflections, because each subcarrier transmits a low-rate sequence that remains unaffected by dispersion. In contrast to the small indoor attocells, FSO systems communicate over much larger distances and encounter commensurately longer channel impulse responses (CIRs), which is beneficially counteracted by the antidispersion capability of ACO-OFDM, as argued in [21]–[24].

This situation is similar to that of classic RF multiple-input multiple-output (MIMO) systems, which require multiple RF chains. Due to the system-level similarity between RF MIMO systems and FSO MTRA systems, the philosophy of antenna selection (AS) techniques originally conceived for conventional RF MIMO systems [25]–[27] may also be applied to FSO MTRA systems, leading to the concept of "aperture selection" (ApS) [28]–[31], which inherits the low cost and low complexity benefits from the classic RF AS. In [28], the concept of transmit selection is first introduced in FSO communication, and it was proved capable of achieving full diversity, whereas selection at both the transmit and receive sides for multielement FSO is comprehensively studied in [29]. In [30], a practical application of ApS in mobile FSO nodes is exhibited; furthermore, as an extension of ApS, the relay selection based on channel information is described in [31]. Hence, in FSO MTRA systems, given the fixed number of optical chains,[1] employing ApS is capable of significantly improving the system's achievable performance. Furthermore, as the average channel variance increases with the turbulence level of the FSO channel, adopting ApS in FSO MTRA systems becomes beneficial, since the specific links exhibiting the highest power will be activated.

Against the given background, in this paper, we propose a novel ACO-OFDM-based [18]–[20] FSO MTRA system relying on joint ApS for transmission over FSO turbulence channels,[2] which employs joint maximum likelihood (ML)

[1] In this case, we define an entire set of electronic hardware components at the transmit/receive end, including electronic-to-optical conversion or optical-to-electronic conversion, as an optical chain.

[2] Note that the proposed ApS scheme is applicable to any arbitrary OFDM-based system. However, for simplicity of exposition but without any loss of generality, we only use ACO-OFDM in this paper.

hard detection (HD) for uncoded systems and joint maximum *a posteriori* probability (MAP) soft detection (SD) for forward error correction (FEC)-coded systems. Our contributions are as follows.

- We construct a novel ACO-OFDM-based MTRA system and investigate its performance using different detection schemes. We will demonstrate that the resultant BER curves corresponding to different levels of turbulence reveal an intriguing curve-crossing phenomenon.
- We design a novel ApS scheme based on exploiting the FSO channel characteristics for assisting our ACO-OFDM-based MTRA system, which is capable of significantly improving both the achievable BER and throughput, while imposing reduced power consumption and hardware complexity. We will show that the performance gain of our ApS scheme becomes more significant under hostile turbulence channel conditions.

This paper is organized as follows. Section II introduces our ACO-OFDM-based MTRA optical wireless (OW) system designed for the FSO turbulence channels, whereas Section III details the joint ApS scheme proposed for effectively exploiting the system's available optical chains. Both BER performance and extrinsic information transfer (EXIT) chart-based throughput analysis of our system are presented in Section IV. Our conclusions are summarized in Section V.

Throughout our discussions, $(\ )^{\mathrm{T}}$ and $(\ )^{\mathrm{H}}$ denote the transpose and conjugate transpose operators, respectively, whereas $(\ )^{-1}$ and $(\ )^{*}$ stand for the inverse and conjugate operations, respectively. $\boldsymbol{I}$ denotes the identity matrix with an appropriate dimension. Under the MTRA context, we have the N_t transmit apertures (TAps) at the transmitter and the N_r receive apertures (RAps) at the receiver. Additionally, $\mathbb{T}(\cdot)$ denotes the composite SD-decoding transfer function.

II. Asymmetrically Clipped Optical Orthogonal Frequency Division Multiplexing-Based Multiple Transmit/Receive Aperture System

A. ACO-OFDM

The ACO-OFDM input vector of the mth MTRA substream $0 \leq m \leq M-1$ is constituted by the $N_F/4$ frequency domain (FD) data symbols given by $\boldsymbol{S}_{ACO}^{(m)} = [S_0^{(m)}\ S_1^{(m)}\ \cdots\ S_{N_F/4-1}^{(m)}]^{\mathrm{T}}$, where M is the total number of optical chains, and N_F represents the length of OFDM symbols. Quadrature amplitude modulation (QAM) signaling is employed. ACO-OFDM only uses the odd-indexed subcarriers to carry data while assigning "0's" to the even-indexed subcarriers as well as simultaneously adopting a Hermitian-symmetric symbol arrangement. Thus, $\boldsymbol{S}_{ACO}^{(m)}$ is first expanded into the following form:

$$\begin{aligned}\boldsymbol{S}^{(m)} &= \left[0\ S_0^{(m)}\ \cdots\ 0\ S_{N_F/4-1}^{(m)}\ 0\ \left(S_{N_F/4-1}^{(m)}\right)^*\ \cdots\ 0\ \left(S_0^{(m)}\right)^*\right]^{\mathrm{T}}\\ &= \left[\bar{S}_0^{(m)}\ \bar{S}_1^{(m)}\ \cdots\ \bar{S}_{N_F-1}^{(m)}\right]^{\mathrm{T}}. \end{aligned} \tag{1}$$

By defining the N_F-point inverse fast Fourier transform matrix as

$$\boldsymbol{F} = \frac{1}{\sqrt{N_F}}\begin{bmatrix} 1 & 1 & \cdots & 1\\ 1 & e^{\mathrm{j}2\pi/N_F} & \cdots & e^{\mathrm{j}2\pi(N_F-1)/N_F}\\ \vdots & \vdots & \ddots & \vdots\\ 1 & e^{\mathrm{j}2\pi(N_F-1)/N_F} & \cdots & e^{\mathrm{j}2\pi(N_F-1)^2/N_F}\end{bmatrix} \tag{2}$$

where $\mathrm{j} = \sqrt{-1}$, the time domain (TD) OFDM symbol vector is given by

$$\boldsymbol{s}^{(m)} = \left[s_0^{(m)}\ s_1^{(m)}\ \cdots\ s_{N_F-1}^{(m)}\right]^{\mathrm{T}} = \boldsymbol{F}\boldsymbol{S}^{(m)}. \tag{3}$$

All the negative-valued elements in $\boldsymbol{s}^{(m)}$ are forced to become zero by the clipping operation. As a benefit of this ACO-OFDM modulation arrangement, the useful odd-indexed subcarriers are protected from the detrimental effects of clipping noise. Consequently, the real and imaginary information of the original FD data in $\boldsymbol{S}^{(m)}$, which are spread along all the TD OFDM symbols, is well preserved. After concatenating the N_{cp}-length cyclic prefix (CP) to $\boldsymbol{s}^{(m)}$, the resultant $(N_F + N_{cp})$-length vector $\boldsymbol{s}_o^{(m)}$ is converted into the optical signal by the electronic-to-optical (E/O) converter for transmission.

At the receiver end, after the optical-to-electronic (O/E) conversion and the removal of the CP, the N_F-length TD signal vector received by the nth receiver chain is given by

$$\boldsymbol{y}^{(n)} = R \cdot \bar{\mathbf{H}}^{(n,m)}\boldsymbol{s}_o^{(m)} + \mathbf{v}^{(n,m)} \tag{4}$$

where $\bar{\mathbf{H}}^{(n,m)}$ represents the $N_F \times (N_F + N_{cp})$-element linear convolution channel matrix between the mth transmitter and the $n$the receiver, whereas $\mathbf{v}^{(n,m)}$ denotes the TD additive white Gaussian noise (AWGN) vector imposed on the channel linking the mth TAp to the nth RAp, whose elements have zero mean and a variance of σ^2, whereas R [W/A] is the responsivity of the photodiode. Equation (4) is equivalent to

$$\boldsymbol{y}^{(n)} = R \cdot \mathbf{H}^{(n,m)}\boldsymbol{s}^{(m)} + \mathbf{v}^{(n,m)} \tag{5}$$

where $\mathbf{H}^{(n,m)}$ is the circulant convolution channel matrix of $(N_F \times N_F)$ elements [32], i.e.,

$$\mathbf{H}^{(n,m)} = \begin{bmatrix} h_0 & 0 & \cdots & 0 & \cdots & h_2 & h_1\\ h_1 & h_0 & \cdots & \vdots & \cdots & h_3 & h_2\\ \vdots & \vdots & \ddots & 0 & \ddots & \vdots & \vdots\\ h_{\mathrm{N}_{cp}} & h_{\mathrm{N}_{cp}-1} & \cdots & h_0 & \cdots & h_{\mathrm{N}_{cp}-2} & h_{\mathrm{N}_{cp}-1}\\ 0 & h_{\mathrm{N}_{cp}} & \cdots & \vdots & \ddots & \vdots & \vdots\\ \vdots & \vdots & \ddots & h_{\mathrm{N}_{cp}-1} & \cdots & h_0 & 0\\ 0 & 0 & \cdots & h_{\mathrm{N}_{cp}} & \cdots & h_1 & h_0 \end{bmatrix} \tag{6}$$

with each CIR represented by independent random variables obeying the Gamma–Gamma distribution. Furthermore, $R \cdot \mathbf{H}^{(n,m)} = \boldsymbol{F}\boldsymbol{\Lambda}^{(n,m)}\boldsymbol{F}^{\mathrm{H}}$, in which $\boldsymbol{\Lambda}^{(n,m)}$ is the $(N_F \times N_F)$-element diagonal matrix with eigenvalues of $\mathbf{H}^{(n,m)}$ at its diagonal entries. By applying the fast-Fourier-transform-based

TABLE I
COMPARISON BETWEEN RAYLEIGH FADING CHANNEL AND FSO TURBULENCE CHANNEL

	RF Rayleigh channel	FSO turbulence channel
CIR's values	complex	real and positive
main cause	fading	turbulence
pathloss	yes	yes
scattering	yes	yes
CIRs vary with f_d or C_n^2	yes	yes
variance varies with f_d or C_n^2	no	yes

OFDM demodulation to $\boldsymbol{y}^n$, we obtain the received N_F-length FD symbol vector, i.e.,

$$\boldsymbol{Y}_o^{(n)} = \boldsymbol{F}^{\mathrm{H}}\boldsymbol{y}^{(n)} = \boldsymbol{\Lambda}^{(n,m)}\boldsymbol{S}^{(m)} + \boldsymbol{V}^{(n,m)} \tag{7}$$

where the FD channel noise vector $\boldsymbol{V}^{(n,m)} = \boldsymbol{F}^{\mathrm{H}}\mathbf{v}^{(n,m)}$ also obeys the same AWGN distribution as $\mathbf{v}^{(n,m)}$.

Upon collecting all the odd-indexed elements in the first half of $\boldsymbol{Y}_o^{(n)}$ and arranging them in the $N_F/4$-length vector $\boldsymbol{Y}_{ACO}^{(n)}$, we have

$$\boldsymbol{Y}_{ACO}^{(n)} = \boldsymbol{\Lambda}_{ACO}^{(n,m)}\boldsymbol{S}_{ACO}^{(m)} + \boldsymbol{V}_{ACO}^{(n,m)} \tag{8}$$

where $\boldsymbol{\Lambda}_{ACO}^{(n,m)}$ is the $(N_F/4) \times (N_F/4)$-element diagonal matrix representing the first $N_F/4$ odd-indexed elements extracted from the diagonal of $\boldsymbol{\Lambda}^{(n,m)}$, which $\boldsymbol{V}_{ACO}^{(n,m)}$ contains the first $N_F/4$ odd-indexed elements of $\boldsymbol{V}^{(n,m)}$. Clearly, $\boldsymbol{Y}_{ACO}^{(n)}$ constitutes sufficient statistics for estimating $\boldsymbol{S}_{ACO}^{(m)}$.

B. Channel Model

FSO turbulent channels impose numerous detrimental effects, such as path-loss-induced attenuation and scintillation. These adverse effects can be modeled by a Gamma–Gamma distribution [33], where irradiance is characterized by the product of a pair of independent Gamma-distributed random processes. The probability density function (pdf) of the CIR is given by [33]

$$p_{GG}(\gamma) = \frac{2(\alpha\beta)^{\frac{\alpha+\beta}{2}}}{\Gamma(\alpha)\Gamma(\beta)}\gamma^{\frac{\alpha+\beta}{2}-1} \cdot K_{\alpha-\beta}\left(2\sqrt{\alpha\beta\cdot\gamma}\right) \tag{9}$$

where $\Gamma(\cdot)$ denotes the Gamma function, $K_\nu(\cdot)$ is the modified Bessel function of the second kind, and α and β are the pair of parameters controlling the two Gamma functions.

Specifically, α determines the large-scale scattering caused by refractive effects, which results in beam direction deviation, and it is expressed by [33]

$$\alpha = \left\{\exp\left[\frac{0.49\sigma_r^2}{\left(1+0.18d^2+0.56\sigma_r^{12/5}\right)^{7/6}}\right] - 1\right\}^{-1} \tag{10}$$

whereas β is attributed to the diffraction that leads to beam spreading and irradiance fluctuation, which is given by [33]

$$\beta = \left\{\exp\left[\frac{0.51\sigma_r^2\left(1+0.69\sigma_r^{12/5}\right)^{-5/6}}{\left(1+0.9d^2+0.62\sigma_r^{12/5}\right)^{5/6}}\right] - 1\right\}^{-1}. \tag{11}$$

In (10) and (11), $d = \sqrt{kD^2/4L}$, where $k = 2\pi/\lambda$ denotes the number of optical waves with λ being the wavelength, L indicates the physical-link distance between the TAp and the RAp, whereas D is the diameter of the RAp. Furthermore, σ_r^2 is known as the Rytov variance, which directly relates to the optical variance of the FSO channel, and it is given by

$$\sigma_r^2 = 0.5C_n^2 k^{7/6} L^{11/6} \tag{12}$$

where C_n^2 is the refractive index that determines the level of turbulence.

It is worth emphasizing that although C_n^2 plays a similar role in the Gamma–Gamma channel to that of the normalized Doppler frequency f_d in the classic RF Rayleigh fading channel, they also have significant differences, as listed in Table I. Explicitly, in Table I, we can see not only the similar roles played by f_d and C_n^2 in the corresponding channels, but also their differences. Specifically, unlike the RF Rayleigh fading channel, whose variance does not vary with f_d, the variance of the FSO turbulence channel varies with C_n^2. This points to the potential of acquiring a considerable diversity gain by exploiting ApS techniques in FSO MTRA communication, particularly under stronger turbulence. This is because ApS is capable of choosing the channels with higher gains, leading to an enhanced performance in FSO MTRA communication.

C. System Structure

Our proposed ACO-OFDM-based MTRA OW system is shown in Fig. 1, where all the component blocks on the left-hand side of the vertical dashed line represent the electronic hardware and circuits, whereas on the right-hand side of this dashed line, after the E/O and O/E conversions, the signals are transmitted to and received from the corresponding apertures. Additionally, the FEC encoding block and the iterative decoding block are only related to the coded system relying on SD and decoding. The numbers of the available optical chains at the transmitter and the receiver are M and N, respectively. Generally speaking, we aim for $M < N_t$ and $N < N_r$, where the joint ApS module in Fig. 1 selects M transmit apertures from the total of N_t TAps and N receive apertures from the total of N_r RAps to form an actual $(M \times N)$-element MTRA OW system for communication. In the special case of $M = N_t$ and $N = N_r$, this joint ApS module is not required. For the time being, we assume $M = N_t$ and $N = N_r$ since this is sufficient for us to describe all the components of the system shown in Fig. 1, except for the joint ApS module. Furthermore, the system in Fig. 1 is capable of adopting any MTRA scheme.

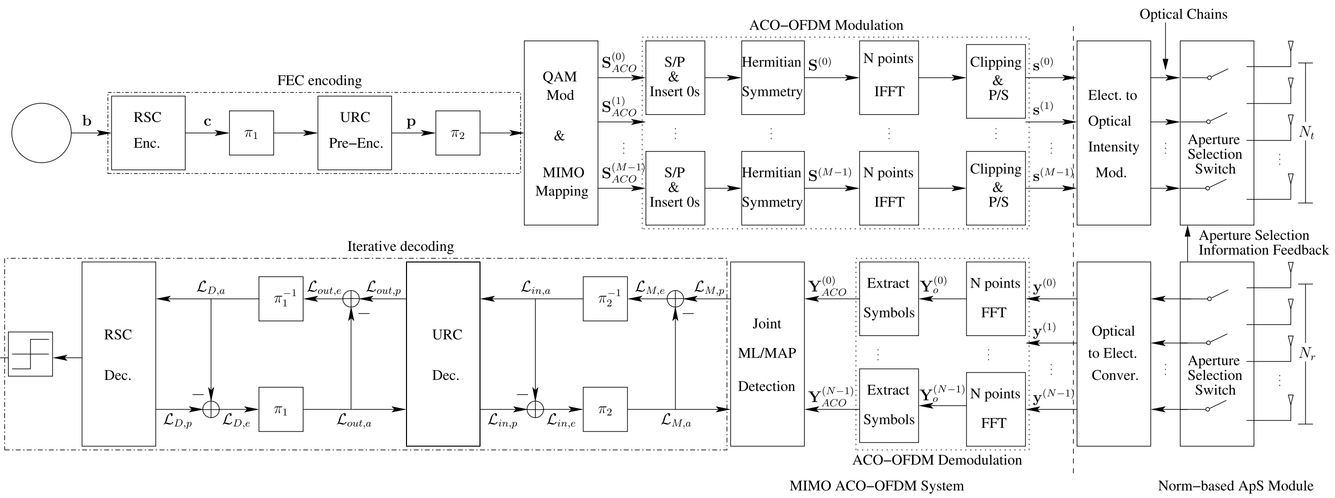

Fig. 1. Schematic of the proposed ACO-OFDM-based MTRA system with the aid of the joint ApS, where M and N are the numbers of optical chains at the transmitter and the receiver, respectively, whereas N_t and N_r are the numbers of transmit and receive apertures, respectively. In general, we have $M < N_t$ and $N < N_r$.

Without loss of generality, in this paper, we will mainly consider the space–time block code (STBC) philosophy [34].

1) Uncoded Joint ML-Based HD System: As shown in Fig. 1, the original information bits, which are denoted as $\boldsymbol{b}$, are first modulated into the $N_F/4$-length QAM symbol vector denoted by $\boldsymbol{X} = [X_0\ X_1\ \cdots\ X_{N_F/4-1}]^{\mathrm{T}}$, which is then mapped onto the M substreams of $\boldsymbol{S}_{ACO}^{(m)}$ for $0 \leq m \leq M-1$, according to the STBC MTRA scheme, i.e.,

$$\boldsymbol{S}_{ACO} = \mathcal{F}_{\mathrm{STBC}}(\boldsymbol{X}) \tag{13}$$

relying on the STBC mapping $\mathcal{F}_{\mathrm{STBC}}(\cdot)$. Taking the G2 STBC scheme $(M=2)$ as an example, the two rows of $\boldsymbol{S}_{ACO}$ are given by $\boldsymbol{S}_{ACO}^{(0)} = (1/\sqrt{M})[X_0\ -X_1^*\ \cdots\ X_{N_F/4-2}\ -X_{N_F/4-1}^*]^{\mathrm{T}}$ and $\boldsymbol{S}_{ACO}^{(1)} = (1/\sqrt{M})[X_1\ -X_0^*\ \cdots\ X_{N_F/4-1}\ -X_{N_F/4-2}^*]^{\mathrm{T}}$. Each $\boldsymbol{S}_{ACO}^{(m)}$ is processed by an ACO-OFDM modulator to generate the TD unipolar signal vector $\boldsymbol{s}^{(m)}$, as detailed in Section II-A. After optical intensity modulation, $\boldsymbol{s}^{(m)}$ is launched through the mth TAp associated with the mth optical chain of the transmitter.

The M signal substreams are transmitted over the $(N \times M)$-element MTRA FSO turbulence channel, having the characteristics described in Section II-B. At the receiver, after O/E, the N received TD signal substreams $\boldsymbol{y}^{(n)}$ for $0 \leq n \leq N-1$ are passed through the ACO-OFDM demodulator to extract the useful complex-valued sequences $\boldsymbol{Y}_{ACO}^{(n)}$ for $0 \leq n \leq N-1$. Assuming that perfect knowledge of channel state information (CSI) is known at the receiver, the joint ML detection of $\boldsymbol{X}$ can be carried out given $\boldsymbol{Y}_{ACO}^{(n)}$ for $0 \leq n \leq N-1$, which is denoted as $\widehat{\boldsymbol{X}}$. Finally, the estimate of the transmitted binary bit block $\boldsymbol{b}$, which is denoted as $\widehat{\boldsymbol{b}}$, can be obtained by QAM demapping of the ML estimate $\widehat{\boldsymbol{X}}$.

More specifically, upon collecting all the received $\boldsymbol{Y}_{ACO}^{(n)}$ for $0 \leq n \leq N-1$ in the $(N \cdot N_F/4)$-length vector, we have: $\boldsymbol{Y}_{ACO} = [(\boldsymbol{Y}_{ACO}^{(0)})^{\mathrm{T}}\ (\boldsymbol{Y}_{ACO}^{(1)})^{\mathrm{T}}\ \cdots\ (\boldsymbol{Y}_{ACO}^{(N-1)})^{\mathrm{T}}]^{\mathrm{T}}$. Then, according to (8), $\boldsymbol{Y}_{ACO}$ can be expressed as

$$\boldsymbol{Y}_{ACO} = \boldsymbol{\Lambda}_{ACO}\boldsymbol{S}_{ACO} + \boldsymbol{V}_{ACO} \tag{14}$$

in which $\boldsymbol{V}_{ACO} = [(\boldsymbol{V}_{ACO}^{(0)})^{\mathrm{T}}\ (\boldsymbol{V}_{ACO}^{(1)})^{\mathrm{T}}\ \cdots\ (\boldsymbol{V}_{ACO}^{(N-1)})^{\mathrm{T}}]^{\mathrm{T}}$ with $\boldsymbol{V}_{ACO}^{(n)} = \sum_{m=0}^{M-1} \boldsymbol{V}_{ACO}^{(n,m)}$, whereas $\boldsymbol{S}_{ACO} = [(\boldsymbol{S}_{ACO}^{(0)})^{\mathrm{T}}\ (\boldsymbol{S}_{ACO}^{(1)})^{\mathrm{T}}\ \cdots\ (\boldsymbol{S}_{ACO}^{(M-1)})^{\mathrm{T}}]^{\mathrm{T}}$, and

$$\boldsymbol{\Lambda}_{ACO} = \begin{bmatrix} \boldsymbol{\Lambda}_{ACO}^{(0,0)} & \boldsymbol{\Lambda}_{ACO}^{(0,1)} & \cdots & \boldsymbol{\Lambda}_{ACO}^{(0,M-1)} \\ \boldsymbol{\Lambda}_{ACO}^{(1,0)} & \boldsymbol{\Lambda}_{ACO}^{(1,1)} & \cdots & \boldsymbol{\Lambda}_{ACO}^{(1,M-1)} \\ \vdots & \vdots & \vdots & \vdots \\ \boldsymbol{\Lambda}_{ACO}^{(N-1,0)} & \boldsymbol{\Lambda}_{ACO}^{(N-1,1)} & \cdots & \boldsymbol{\Lambda}_{ACO}^{(N-1,M-1)} \end{bmatrix}. \tag{15}$$

Therefore, the ML estimate $\widehat{\boldsymbol{X}}$ is the solution to the following optimization problem:

$$\widehat{\boldsymbol{X}} = \arg\min_{\widetilde{\boldsymbol{X}} \in \mathbb{X}} \left\| \boldsymbol{Y}_{ACO} - \boldsymbol{\Lambda}_{ACO}\mathcal{F}_{\mathrm{STBC}}\left(\widetilde{\boldsymbol{X}}\right) \right\|^2 \tag{16}$$

where $\mathbb{X}$ denotes the feasible set of $\boldsymbol{X}$, i.e., $\boldsymbol{X}$ assumes a value from the set $\mathbb{X}$, and the size of $\mathbb{X}$ is $\zeta^{N_F/4}$ for the ζ-QAM signaling.

Note that there is a total of $(N_r \times N_t)$ FSO turbulence channels, and the overall MTRA channel matrix can be expressed as

$$\mathbf{H} = \begin{bmatrix} \mathbf{H}^{(0,0)} & \mathbf{H}^{(0,1)} & \cdots & \mathbf{H}^{(0,N_t-1)} \\ \mathbf{H}^{(1,0)} & \mathbf{H}^{(1,1)} & \cdots & \mathbf{H}^{(1,N_t-1)} \\ \vdots & \vdots & \vdots & \vdots \\ \mathbf{H}^{(N_r-1,0)} & \mathbf{H}^{(N_r-1,1)} & \cdots & \mathbf{H}^{(N_r-1,N_t-1)} \end{bmatrix}. \tag{17}$$

According to (5), the corresponding overall MTRA channel model is then given by

$$\boldsymbol{y} = R \cdot \mathbf{H}\boldsymbol{s} + \mathbf{V} \tag{18}$$

where we have $\boldsymbol{y} = [(\boldsymbol{y}^{(0)})^{\mathrm{T}}\ (\boldsymbol{y}^{(1)})^{\mathrm{T}}\ \cdots\ (\boldsymbol{y}^{(N_r-1)})^{\mathrm{T}}]^{\mathrm{T}}$, and $\boldsymbol{s} = [(\boldsymbol{s}^{(0)})^{\mathrm{T}}\ (\boldsymbol{s}^{(1)})^{\mathrm{T}}\ \cdots\ (\boldsymbol{s}^{(N_t-1)})^{\mathrm{T}}]^{\mathrm{T}}$, whereas the noise matrix $\mathbf{V} = [(\mathbf{V}^{(0)})^{\mathrm{T}}\ (\mathbf{V}^{(1)})^{\mathrm{T}}\ \cdots\ (\mathbf{V}^{(N_r-1)})^{\mathrm{T}}]^{\mathrm{T}}$ cc $\mathbf{V}^{(n)} = \sum_{m=0}^{N_t-1} \mathbf{V}^{(n,m)}, 0 \leq n \leq N_r - 1$. To support such a large-scale MTRA system, we need $M = N_t$ optical chains at the transmitter and $N = N_r$ optical chains at the receiver, which is costly.

2) Three-Stage Iterative Joint MAP-Based SD System: The information bit sequence $\boldsymbol{b}$ is first channel encoded by a half-rate recursive systematic code (RSC)-based outer encoder, yielding the coded bit sequence $\boldsymbol{c}$, which is then bit-interleaved by π_1 in Fig. 1. Furthermore, we invoke a unit-rate code (URC) as the inner encoder, which is associated with the bit-interleaver π_2 in Fig. 1. The explicit benefit of incorporating a low-complexity memory-1 URC is that it allows the system to beneficially spread the *extrinsic* information across the iterative decoder components without increasing its delay, and as a result, a vanishingly low BER is attainable [35]–[37]. Following the two-stage encoding process, the coded bits traverse through the same QAM modulator and STBC MTRA mapper, as described in Section II-C1.

The corresponding three-stage turbo decoder of the receiver is also shown in Fig. 1, which consists of a joint MAP-based SD, a URC decoder, and an RSC decoder. More explicitly, the composite inner decoder is formed by the combined joint MAP-based SD and the URC decoder, where the associated *a priori* information and *extrinsic* information are first interleaved and exchanged I_{inner} times. The outer decoder is constituted by the RSC decoder, where the information gleaned from the inner decoder is iteratively exchanged I_{outer} times. The final HD is then carried out by the RSC decoder to produce the estimate $\widehat{\boldsymbol{b}}$ of the transmitted information bit block $\boldsymbol{b}$.

For ease of explanation, the information exchanged between the decoder components, in terms of log-likelihood ratios (LLRs) [37] as shown in Fig. 1, is first defined.

- $\mathcal{L}_{M,p}$, $\mathcal{L}_{M,a}$, $\mathcal{L}_{M,e}$: the *a posteriori*, *a priori*, and *extrinsic* LLRs, respectively, associated with the joint MAP-based SD block, which are detailed in [35] and [38].
- $\mathcal{L}_{in,p}$, $\mathcal{L}_{in,a}$, $\mathcal{L}_{in,e}$: the *a posteriori*, *a priori*, and *extrinsic* LLRs, respectively, associated with the URC decoder block.
- $\mathcal{L}_{out,p}$, $\mathcal{L}_{out,a}$, $\mathcal{L}_{out,e}$: the *a posteriori*, *a priori*, and *extrinsic* LLRs, respectively, associated with the composite inner decoder block.
- $\mathcal{L}_{D,p}$, $\mathcal{L}_{D,a}$, $\mathcal{L}_{D,e}$: the *a posteriori*, *a priori*, and *extrinsic* LLRs, respectively, associated with the outer RSC decoder block.

Since the ζ-QAM scheme maps a set of $\eta = \log_2 \zeta$ consecutive incoming bits onto a symbol value, we consider a set of $\boldsymbol{p}_{(1:\eta)} = \{p_1, p_2, \ldots, p_\eta\}$ consecutive bits without loss of generality. For the vth bit of $\boldsymbol{p}_{(1:\eta)}$, its bitwise *a posteriori* LLR can be derived by the classic Max-Log approximation [35] as

$$\begin{aligned}\mathcal{L}_{M,p}(p_v)& \\ = \mathcal{L}_{M,a}(p_v)& \\ + \max_{\widetilde{\boldsymbol{X}}\in\mathbb{X}_1^{p_v}} &\left\{-\left\|\boldsymbol{Y}_{ACO} - \boldsymbol{\Lambda}_{ACO}\mathcal{F}_{\text{STBC}}(\widetilde{\boldsymbol{X}})\right\|^2 \Big/ 2\sigma^2 + A\right\} \\ - \max_{\widetilde{\boldsymbol{X}}\in\mathbb{X}_0^{p_v}} &\left\{\left\|\boldsymbol{Y}_{ACO} - \boldsymbol{\Lambda}_{ACO}\mathcal{F}_{\text{STBC}}(\widetilde{\boldsymbol{X}})\right\|^2 \Big/ 2\sigma^2 + A\right\}\end{aligned} \tag{19}$$

where we have $A = \sum_{\tau=1,\tau\neq v}^{\eta} p_v \mathcal{L}_{M,a}(p_\tau)$, whereas $\mathbb{X}_0^{p_v} = \{\widetilde{\boldsymbol{X}} \in \mathbb{X} | p_v = 0\}$ and $\mathbb{X}_1^{p_v} = \{\widetilde{\boldsymbol{X}} \in \mathbb{X} | p_v = 1\}$. The *extrinsic* LLRs $\mathcal{L}_{M,e}$ gleaned from the joint MAP-based SD block are deinterleaved, and then, they are fed as the *a priori* LLRs $\mathcal{L}_{in,a}$ into the URC predecoder in Fig. 1, which, in turn, calculates its *a posteriori* LLRs $\mathcal{L}_{in,p}$. Then, the updated *extrinsic* LLRs $\mathcal{L}_{in,e}$ are fed back and reinterleaved, before being processed as the *a priori* LLRs $\mathcal{L}_{M,a}$ by the SD block in the next inner iteration [35]–[37]. After the convergence of the inner iteration process after I_{in} iterations, the outer iteration follows a similar procedure, which involves exchanging the corresponding *extrinsic* LLRs between the URC decoder and the RSC decoder, until the predefined stopping criterion, which is specified by the number of outer iterations I_{out}, is met.

III. Proposed Joint Aperture Selection Scheme

In practice, the number of available optical chains is limited, and typically, we have $M \ll N_t$ and $N \ll N_r$. To most efficiently exploit the available optical chains, it is highly desirable to select the most appropriate subset of the $N \times M$ FSO links from the full set of the $N_r \times N_t$ channels for the ACO-OFDM-based MTRA system having only M optical chains at the transmitter and N optical chains at the receiver. In other words, the task is to select M appropriate TAps as well as N appropriate RAps from the total of N_t TAps and the total of N_r RAps, respectively, to form the most beneficial $(N \times M)$-element subset MTRA channel matrix for actual communication. The ApS module in Fig. 1 is responsible for carrying out this task, and we adopt a low-complexity yet efficient ApS scheme.

A generic $(N \times M)$-element subset MTRA channel matrix $\mathbf{H}_{\text{sub}} \subset \mathbf{H}$, where $\mathbf{H}$ is the full $(N_r \times N_t)$ MTRA channel matrix of (17), can be formulated as

$$\mathbf{H}_{\text{sub}} = \begin{bmatrix} \mathbf{H}^{(i_0,j_0)} & \mathbf{H}^{(i_0,j_1)} & \cdots & \mathbf{H}^{(i_0,j_{M-1})} \\ \mathbf{H}^{(i_1,j_0)} & \mathbf{H}^{(i_1,j_1)} & \cdots & \mathbf{H}^{(i_1,j_{M-1})} \\ \vdots & \vdots & \vdots & \vdots \\ \mathbf{H}^{(i_{N-1},j_0)} & \mathbf{H}^{(i_{N-1},j_1)} & \cdots & \mathbf{H}^{(i_{N-1},j_{M-1})} \end{bmatrix} \tag{20}$$

where we have

$$\begin{aligned} 0 \le i_0 < i_1 < \cdots < i_{N-1} \le N_r - 1 \\ 0 \le j_0 < j_1 < \cdots < j_{M-1} \le N_t - 1. \end{aligned} \tag{21}$$

Generally speaking, a higher channel gain yields a better system performance. This leads to the joint ApS approach, which selects the specific TAps and RAps related to the particular subset channel matrix associated with the highest channel norm. Since the FSO channels are characterized by real and positive coefficients, the original norm operation applied to $\mathbf{H}^{(i_r,j_t)}$ can be omitted, which further reduces the complexity imposed. Hence, the subset channel matrix $\mathbf{H}_{\text{sub}}^{\text{opt}}$ based on the joint ApS criterion is found by solving the following optimization problem:

$$\mathbf{H}_{\text{sub}}^{\text{opt}} = \arg\max_{\mathbf{H}_{\text{sub}}\subset\mathbf{H}} \sum_{t=0}^{M-1}\sum_{r=0}^{N-1} \left\|\mathbf{H}^{(i_r,j_t)}\right\|^2. \tag{22}$$

Owing to the specific block-diagonal structure of the full MTRA channel matrix $\mathbf{H}$, the summation in (22) is over the block-diagonal matrices $\mathbf{H}^{(i_r,j_t)}$. Solving the optimization of (22) by exhaustive search requires the evaluation of the norms of $(\mathsf{C}_{N_r}^N \times \mathsf{C}_{N_t}^M)$ candidate subset matrices, where $\mathsf{C}_k^n = k!/(n!(k-n)!)$, and $\mathsf{C}_{N_r}^N$ and $\mathsf{C}_{N_t}^M$ are the "row"-block-dimension and "column"-block-dimension combinations of $\mathbf{H}_{\text{sub}}$, respectively. By adopting the aforementioned strategy along with the process to be detailed below in Section III, our joint ApS scheme solves the optimization of (22) at significantly reduced complexity.

Given the full channel matrix $\mathbf{H}$ of (17), without loss of generality, let us assume $\mathsf{C}_{N_r}^N < \mathsf{C}_{N_t}^M$. The joint ApS algorithm accomplishes the optimization in the following two steps.

Step 1): "Row"-Block Dimension Operations: Let $n_r \in \{1, 2, \ldots, \mathsf{C}_{N_r}^N\}$ be the "row"-block combination index, and the "row"-block indexes corresponding to the n_rth candidate submatrix $\mathbf{H}_{n_r}$ of N row blocks and N_t column blocks be given by

$$\boldsymbol{l}_{n_r} = \left[l_{n_r}^0 \ l_{n_r}^1 \ \cdots \ l_{n_r}^{N-1}\right]^{\mathrm{T}}. \tag{23}$$

Then, the n_rth "row"-block-based candidate submatrix $\mathbf{H}_{n_r}$ is given by

$$\mathbf{H}_{n_r} = \begin{bmatrix} \mathbf{H}^{\left(l_{n_r}^0,0\right)} & \mathbf{H}^{\left(l_{n_r}^0,1\right)} & \cdots & \mathbf{H}^{\left(l_{n_r}^0,N_t-1\right)} \\ \mathbf{H}^{\left(l_{n_r}^1,0\right)} & \mathbf{H}^{\left(l_{n_r}^1,1\right)} & \cdots & \mathbf{H}^{\left(l_{n_r}^1,N_t-1\right)} \\ \vdots & \vdots & \vdots & \vdots \\ \mathbf{H}^{\left(l_{n_r}^{N-1},0\right)} & \mathbf{H}^{\left(l_{n_r}^{N-1},1\right)} & \cdots & \mathbf{H}^{\left(l_{n_r}^{N-1},N_t-1\right)} \end{bmatrix}. \tag{24}$$

Computing

$$m_{n_r}^x = \sum_{i=0}^{N-1} \left\| \mathbf{H}^{\left(l_{n_r}^i,x\right)} \right\|^2, \quad 0 \le x \le N_t - 1 \tag{25}$$

where $m_{n_r}^x$ represents the square norm of the xth column block in $\mathbf{H}_{n_r}$, yields the norm metric vector, i.e.,

$$\mathbf{m}_{n_r}^{\mathrm{T}} = \left[m_{n_r}^0 \ m_{n_r}^1 \ \cdots \ m_{n_r}^{N_t-1}\right]. \tag{26}$$

Applying (26) to all the $\mathsf{C}_{N_r}^N$ possible combinations leads to the $(\mathsf{C}_{N_r}^N \times N_t)$-element norm metric matrix $\mathbf{M}$ given by

$$\mathbf{M} = \begin{bmatrix} \mathbf{m}_1^{\mathrm{T}} \\ \mathbf{m}_2^{\mathrm{T}} \\ \vdots \\ \mathbf{m}_{\mathsf{C}_{N_r}^N}^{\mathrm{T}} \end{bmatrix} = \begin{bmatrix} m_1^0 & m_1^1 & \cdots & m_1^{N_t-1} \\ m_2^0 & m_2^1 & \cdots & m_2^{N_t-1} \\ \vdots & \vdots & \cdots & \vdots \\ m_{\mathsf{C}_{N_r}^N}^0 & m_{\mathsf{C}_{N_r}^N}^1 & \cdots & m_{\mathsf{C}_{N_r}^N}^{N_t-1} \end{bmatrix}. \tag{27}$$

Step 2): "Column"-Block Dimension Operations: Find the largest M elements in the n_rth row of $\mathbf{M}$ and sum them up, which is denoted as $m_{\max}^{n_r}$, as well as record the column-block indexes of these M blocks in the index vector, i.e.,

$$\boldsymbol{l}_{n_c}(n_r) = \left[l_{n_c}^0(n_r) \ l_{n_c}^1(n_r) \ \cdots \ l_{n_c}^{M-1}(n_r)\right]^{\mathrm{T}}. \tag{28}$$

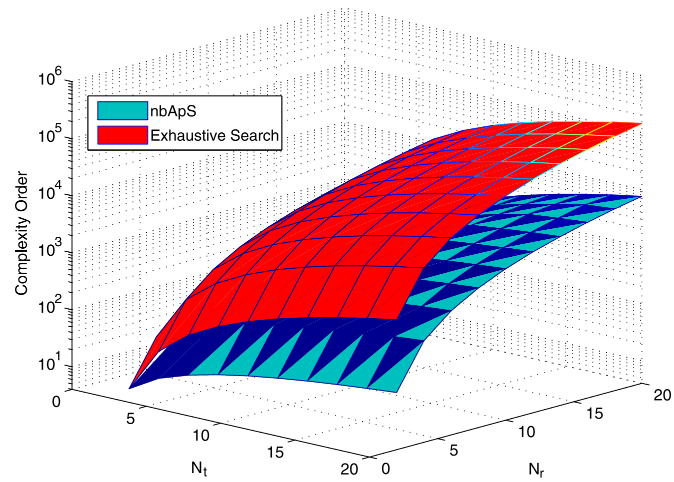

Fig. 2. Complexity comparison of our joint ApS and exhaustive search method, where the number of optical chains at the transmit and receive sides is $M = N = 2$.

This produces the max-norm metric vector, i.e.,

$$\mathbf{m}_{\max}^{\mathrm{T}} = \left[m_{\max}^1 \ m_{\max}^2 \ \cdots \ m_{\max}^{\mathsf{C}_{N_r}^N}\right]. \tag{29}$$

Next, find

$$\bar{n}_r = \arg \max_{1 \le n_r \le \mathsf{C}_{N_r}^N} m_{\max}^{n_r}. \tag{30}$$

Then, the selected TAp and RAp indexes are specified by $\boldsymbol{l}_{n_c}(\bar{n}_r)$ and $\boldsymbol{l}_{\bar{n}_r}$, respectively, and the corresponding subset channel matrix $\mathbf{H}_{\text{sub}}$ is the optimal solution of (22). In other words, we have the solution of the optimization problem (22) given by

$$\mathbf{H}_{\text{sub}}^{\text{opt}} = \begin{bmatrix} \mathbf{H}^{\left(l_{\bar{n}_r}^0, l_{n_c}^0(\bar{n}_r)\right)} & \mathbf{H}^{\left(l_{\bar{n}_r}^0, l_{n_c}^1(\bar{n}_r)\right)} & \cdots & \mathbf{H}^{\left(l_{\bar{n}_r}^0, l_{n_c}^{M-1}(\bar{n}_r)\right)} \\ \mathbf{H}^{\left(l_{\bar{n}_r}^1, l_{n_c}^0(\bar{n}_r)\right)} & \mathbf{H}^{\left(l_{\bar{n}_r}^1, l_{n_c}^1(\bar{n}_r)\right)} & \cdots & \mathbf{H}^{\left(l_{\bar{n}_r}^1, l_{n_c}^{M-1}(\bar{n}_r)\right)} \\ \vdots & \vdots & \vdots & \vdots \\ \mathbf{H}^{\left(l_{\bar{n}_r}^{N-1}, l_{n_c}^0(\bar{n}_r)\right)} & \mathbf{H}^{\left(l_{\bar{n}_r}^{N-1}, l_{n_c}^1(\bar{n}_r)\right)} & \cdots & \mathbf{H}^{\left(l_{\bar{n}_r}^{N-1}, l_{n_c}^{M-1}(\bar{n}_r)\right)} \end{bmatrix}. \tag{31}$$

The complexity of this joint ApS on the order of $C_{\text{nbApS}} \approx \mathcal{O}((N_t \cdot N) \cdot \mathsf{C}_{N_r}^N)$, which is much lower than that of the exhaustive search $C_{\text{ES}} \approx \mathcal{O}((N \cdot M) \cdot (\mathsf{C}_{N_t}^M \cdot \mathsf{C}_{N_r}^N))$. If we have $\mathsf{C}_{N_r}^N > \mathsf{C}_{N_t}^M$, the joint ApS starts with **Step 1**) constituted now by the "Column"-Block Dimension Operations followed by **Step 2**), which is now represented by the "Row"-Block Dimension Operations. The complexity of this algorithm is $\mathcal{O}((N_r \cdot M) \cdot \mathsf{C}_{N_t}^M)$. Based on this estimation, the complexity of these two methods is shown in Fig. 2; we may observe that the complexity of our proposed algorithm is profoundly lower than the complexity obtained from the exhaustive search method.

Since N and M are the numbers of available optical chains at the receiver and the transmitter, respectively, and since there are the $N_r \times N_t$ candidate channels, where we have $N_r > N$ and $N_t > M$, we can define the ApS factor as

$$f_{\text{ApS}}(N_t, N_r) = \frac{N_t + N_r}{M + N} \tag{32}$$

which determines the "diversity" order attained by the proposed ACO-OFDM-based MTRA system relying on the joint ApS scheme, in comparison with the $(N \times M)$-element ACO-OFDM-based MTRA system operating without ApS.

IV. Simulation Results

Simulation-based investigations were carried out to evaluate the achievable performance of our ACO-OFDM-based MTRA OW systems, both without ApS and with the aid of the joint ApS. We simulated the turbulent FSO channel within the physical distance of $L = 1000$ m and with the aid of three different refractive index values of $C_n^2 = 4 \times 10^{-15}$, 5×10^{-14}, and 4×10^{-13} to represent all weak, moderate, and strong turbulence levels, respectively. The modulation schemes employed were 4-QAM, and we considered both the G2 and G4 STBC configurations associated with $M = N = 2$ and $M = N = 4$, respectively, whose system throughput values are identical, whereas the OFDM block length was set to $N_F = 512$. The signal-to-noise ratio (SNR) was defined as the ratio of the total transmitted signal power over the total channel noise power.

A. Performance of the Uncoded MTRA System With Joint ML-Based HD

1) System Without ApS: Let us first consider the basic STBC-aided ACO-OFDM MTRA system, where the numbers of TAps and RAps were equal to the numbers of the corresponding transmit and receive optical chains, respectively. Therefore, no ApS was needed. The BER performance of the G2 and G4 STBC-based ACO-OFDM MTRA systems operating without ApS is shown in Fig. 3 for three different channel turbulence levels.

As expected, the system adopting the G4 STBC scheme always outperforms the G2-STBC-scheme-based system given the same channel turbulence level, since the former attains a higher diversity gain. Intuitively, we would expect that the BER curve of the system operating in a strongly turbulent channel would always be above the BER curve of the same system communicating over a weakly turbulent channel. This trend is similar to that observed for the classic STBC systems in RF communication, where the BER obtained in a high-Doppler-shift environment is typically poorer than that of a low-Doppler-shift environment, unless perfect channel estimation is assumed. However, observe the intriguing BER curve-crossing phenomenon shown in Fig. 3. For example, it is shown in Fig. 3 that the BER curve of the G4 STBC system operating in the highly turbulent channel associate with $C_n^2 = 4 \times 10^{-13}$ is actually lower than that of the same G4 STBC system in the weakly turbulent channel of $C_n^2 = 4 \times 10^{-15}$, at SNR < 5 dB. At SNR $= 5$ dB, the two BER curves cross over each other, and the performance of the G4 STBC system operating in the strongly turbulent channel becomes poorer than that communicating over the weakly turbulent channel, for SNR > 5 dB. For the G2 STBC scheme, the BER curve crossover occurs at approximately SNR $= 1$ dB, whereas for the higher-order G4 STBC scheme, the curve-crossing phenomenon is more pronounced, and the crossover takes place in the SNR region of 4–7 dB.

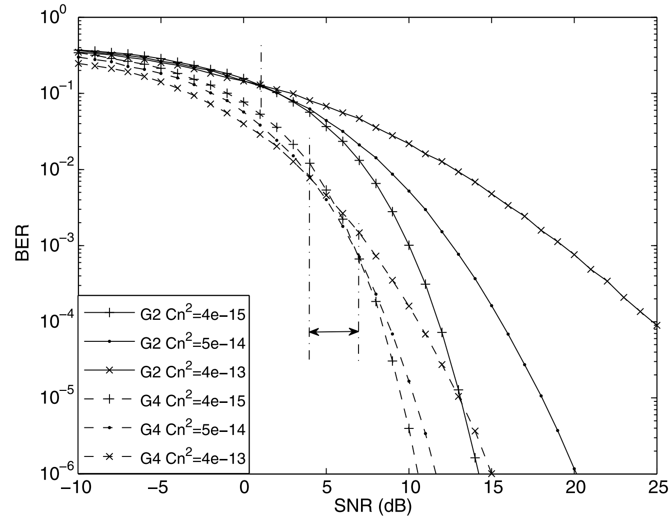

Fig. 3. BER performance of the G2 and G4 STBC-based ACO-OFDM MTRA systems without ApS, communicating over the FSO turbulence channels of weak, moderate, and strong turbulence levels. "Curve crossing" is marked by a dash-dot vertical line.

The question is then why this crossover phenomenon takes place and why it is different from the trends in RF communication. The answer can be found in the comparison made in Table I between the RF fading channel and the FSO turbulence channel. In practical RF communication, changing the Doppler shift only affects the fading rate of the channel, but the variance of the channel's fading envelop remains the same. Therefore, increasing the Doppler frequency of the fading channel typically degrades the BER performance, unless perfect CSI is assumed. By contrast, the FSO turbulent channel is different from the RF fading channel in this aspect. First, indeed, increasing the channel turbulence's level C_n^2 has a detrimental effect on the BER performance, just as increasing the Doppler frequency will impose a detrimental effect on an RF fading channel. However, according to (12), the refractive index C_n^2 also affects the variance of the FSO channel. Thus, changing the turbulence level also affects the channel's pdf. Therefore, unlike in the RF fading channel, the BER curves under different turbulence levels do not start from the same point, and eventually, these curves cross over at some SNR point.

2) System Operating With the Aid of the Joint ApS: We next characterize the BER performance enhancement achieved by the ACO-OFDM MTRA system having $N_r > N$ and $N_t > M$, which relied on the joint ApS in conjunction with various ApS factors, over the original ACO-OFDM MTRA system, given $N_r = N$ and $N_t = M$, which operated without ApS. Since the performance enhancements achieved for the G2 and G4 STBC schemes exhibited the same trend, we only showed the corresponding results for the G2-STBC-based systems, which are shown in Fig. 4.

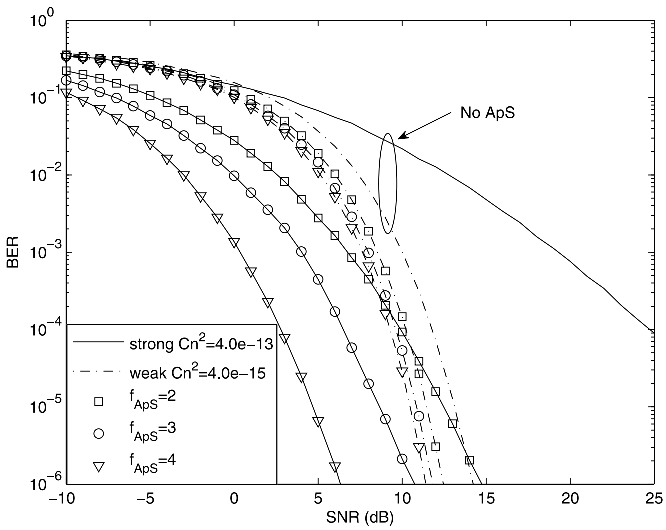

Fig. 4. BER performance enhancement of the G2-STBC-based ACO-OFDM MTRA system with the aid of the joint ApS given three different ApS factors over the original G2-STBC-based ACO-OFDM MTRA system operating without ApS, communicating over the FSO channels of weak and strong turbulence levels.

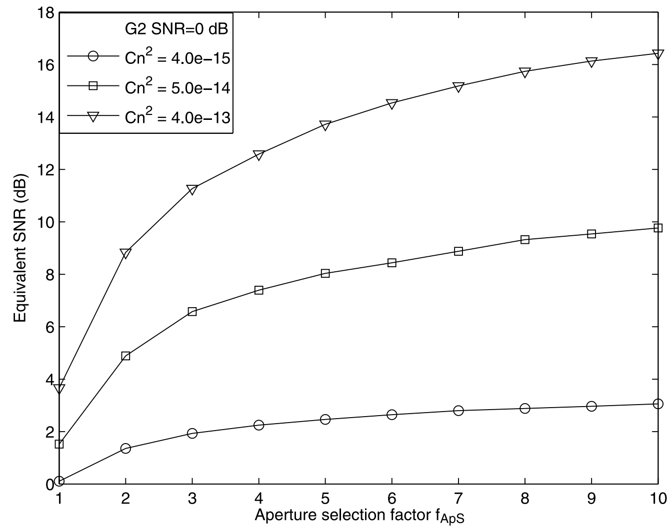

Fig. 5. Equivalent ApS-based SNR as the function of the ApS factor for the G2-STBC-based ACO-OFDM MTRA system with the aid of the joint ApS, under different channel turbulent conditions and given the SNR in the absence of ApS of 0 dB.

It is shown in Fig. 4 that the performance enhancement of the G2-STBC-based ACO-OFDM MTRA system relying on the joint ApS over the original G2-STBC-based ACO-OFDM MTRA system operating without ApS is significantly higher for strongly turbulent channels than for the weakly turbulent channels. This is because in a weakly turbulent channel, the fluctuations of the CIRs remain low, and the envelope differences among all the candidate aperture pairs are relatively small. Therefore, the achievable performance enhancement of ApS is relatively modest. However, in a high-turbulence channel, the fluctuations of the envelop are more dramatical, and the system becomes capable of attaining a much more significant diversity gain. Consequently, more significant performance benefits can be attained by ApS. It can also be observed from Fig. 4 that, for the ApS factors larger than 3, the system's achievable performance under the strongly turbulent channel is actually significantly better than that under weak turbulence. This trend is in stark contrast to that of the original G2-STBC-based ACO-OFDM system operating without ApS. Evidently, the performance gain attained by the proposed joint ApS scheme is more significant under strongly turbulent channel conditions.

3) Equivalent SNR: Intuitively, the diversity gain attained by the joint ApS can be contributed to the carefully selected subset channel matrix of (31), which contains the subset of the specific CIRs having the highest channel gains. Given the system transmit SNR, let us now define the equivalent ApS-based SNR as

$$\mathrm{SNR}_{equ} = 10\log_{10}\left(\frac{\mathrm{SNR}}{MN}\left\|\mathbf{H}_{\mathrm{sub}}^{\mathrm{opt}}\right\|^2\right). \qquad (33)$$

Figs. 5 and 6 portray the increased equivalent ApS-based SNRs versus ApS factor f_{ApS} in the three different turbulent channels, given the actual SNRs in the absence of ApS of 0 and 3 dB, respectively. It is shown in Figs. 5 and 6 that for the strongly turbulent channel, the equivalent ApS-based SNR exhibits the most significant improvement owing to ApS, which is correlated by the substantial BER performance improvement shown in Fig. 4. Furthermore, increasing the ApS factor from 1 to 2 provides the highest increase in the equivalent ApS-based SNR. As expected, if we double the transmit power, the corresponding equivalent ApS-based SNR is increased by about 3 dB, as shown by comparing Figs. 5 and 6.

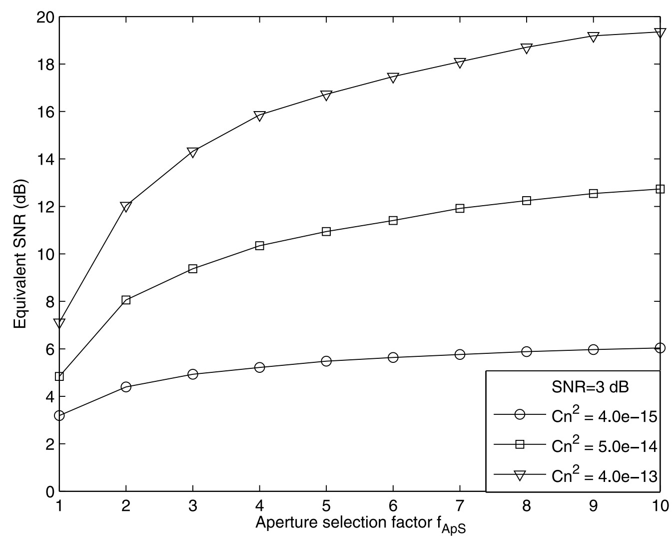

Fig. 6. Equivalent ApS-based SNR as the function of the ApS factor for the G2-STBC-based ACO-OFDM MTRA system with the aid of the joint ApS, under different channel turbulent conditions and given the SNR in the absence of ApS of 3 dB.

B. Performance of the Coded MTRA System With Three-Stage Turbo SD and Decoding

Next, we considered the FEC-coded G2-STBC-based ACO-OFDM MTRA system employing the three-stage iterative joint MAP-based SD and decoding scheme in Fig. 1 presented in Section II-C2. In particular, we investigated the beneficial effects of applying the proposed joint ApS scheme to this coded system. In the simulation study, the generator polynomials of the half-rate RSC encoder were expressed in binary format as $G_{\mathrm{RSC}} = [1, 0, 1]_2$ and $G^r_{\mathrm{RSC}} = [1, 1, 1]_2$, whereas those of the URC encoder were $G_{\mathrm{URC}} = [1, 0]_2$ and $G^r_{\mathrm{URC}} = [1, 1]_2$, where G^r_{RSC} and G^r_{URC} denote the feedback polynomials of the RSC and URC encoders, respectively. The numbers of inner iterations and outer iterations were set to $I_{\mathrm{inner}} = 2$ and $I_{\mathrm{outer}} = 5$. A length of 10^6 bits was used by both system interleavers.

1) EXIT-Chart-Aided Analysis: Having obtained the soft LLRs of the composite inner decoder, let us now invoke the EXIT chart to conveniently analyze the convergence behavior by examining the exchange of the input/output mutual information $I_{out,a}$ and $I_{out,e}$. According to [38], the *extrinsic* mutual information $I_{out,e}$ can be expressed as a function of *a priori* information $I_{out,a}$ and the SNR

$$I_{out,e} = \mathbb{T}(I_{out,a}, \mathrm{SNR}). \tag{34}$$

Furthermore, it has been shown in [38] that the area under the EXIT curve of the composite inner decoder's EXIT chart is approximately equal to the system's normalized achievable throughput $\mathcal{A}$, which is directly related to the SNR by [38]

$$\mathcal{A}(\mathrm{SNR}) = \int_0^1 I_{out,e}\, d\, I_{out,a} = \int_0^1 \mathbb{T}(I_{out,a}, \mathrm{SNR})\, d\, I_{out,a}. \tag{35}$$

Thus, the overall achievable throughput $\mathcal{T}$ can be written as

$$\mathcal{T}(\mathrm{SNR}) = \mathcal{A}(\mathrm{SNR}) \cdot M \cdot \log_2 \zeta. \tag{36}$$

The *a priori* and *extrinsic* mutual information associated with the outer RSC decoder, which is denoted by $I_{D,a}$ and $I_{D,e}$, can also be similarly calculated.

The EXIT curves of the three-stage coded G2-STBC-based ACO-OFDM MTRA system employing the three-stage iterative joint MAP-based SD and decoding scheme communicating over the strongly turbulent channel are shown in Fig. 7. It is shown in Fig. 7 that with the aid of the proposed joint ApS scheme and having an ApS factor of 2, an open EXIT tunnel exists between the EXIT chart curves of the inner SD-URC decoder and the outer RSC decoder at SNR $= -5$ dB. The actual staircase-shaped decoding trajectory is also depicted at SNR $= -5$ dB for this ApS-assisted system, which shows that the point of perfect convergence at (1.0,1.0) can be reached after $I_{\mathrm{outer}} = 5$ iterations. This indicates that this ApS-assisted system is capable of achieving a vanishingly low BER at SNR $= -5$ dB, which is confirmed by the system's BER performance shown in Fig. 10. By contrast, the system operating without ApS fails to achieve an open tunnel between the EXIT chart curves of the inner SD-URC decoder and the outer RSC decoder at SNR $= -5$ dB. This implies that the system operating without ApS cannot achieve perfect decoding at SNR $= -5$ dB, which is confirmed by its BER performance shown in Fig. 10.

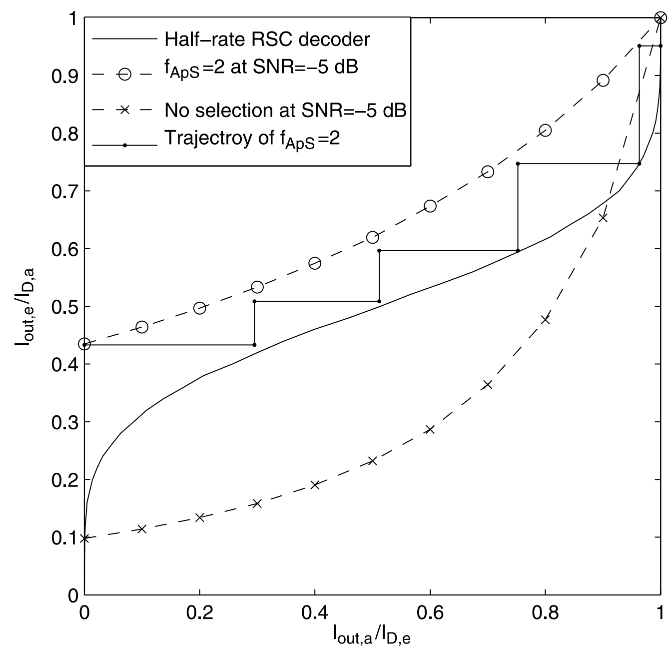

Fig. 7. EXIT characteristics of the three-stage iteratively decoded G2-STBC-based ACO-OFDM MTRA system, communicating over the strongly turbulent channel of $C_n^2 = 4 \times 10^{-13}$ and given the SNR of -5 dB.

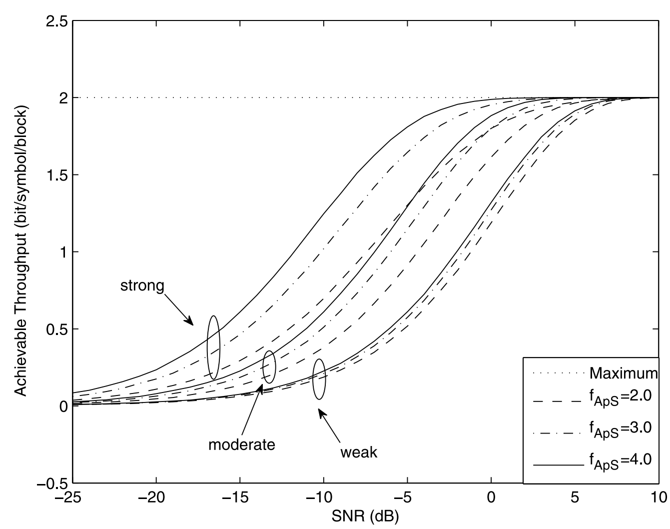

Fig. 8. Achievable throughput values of the three-stage iteratively decoded G2-STBC-based ACO-OFDM MTRA system with the aid of the joint ApS scheme having ApS factors of 2, 3, and 4, communicating over different turbulent channels.

Additionally, according to (36), Fig. 8 portrays the achievable throughput values of our proposed ApS-assisted system having ApS factors of 2, 3, and 4 and communicating over three different turbulent channels. For this system, the maximum achievable throughput is $0.5 \cdot M \cdot \log_2 \zeta = 2$ [bits/symbol/block]. It can be observed from Fig. 8 that for higher ApS factors and for stronger turbulence, a higher throughput is attained for a given SNR value or, equivalently, a lower SNR is required for reaching a given throughput. The results in Fig. 8 clearly indicate that the performance improvement attained by the proposed joint ApS scheme

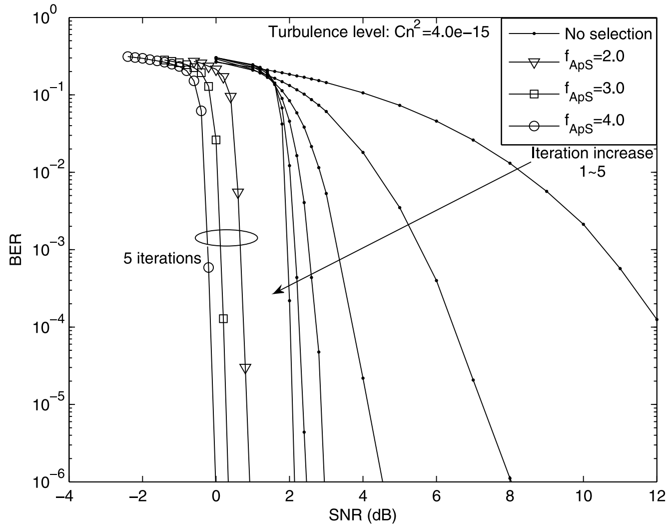

Fig. 9. BER performance comparison of the three-stage iteratively decoded G2-STBC-based ACO-OFDM MTRA systems employing the joint ApS scheme having ApS factors of 2, 3, and 4, respectively, as well as operating without ApS, communicating over the weakly turbulent channel.

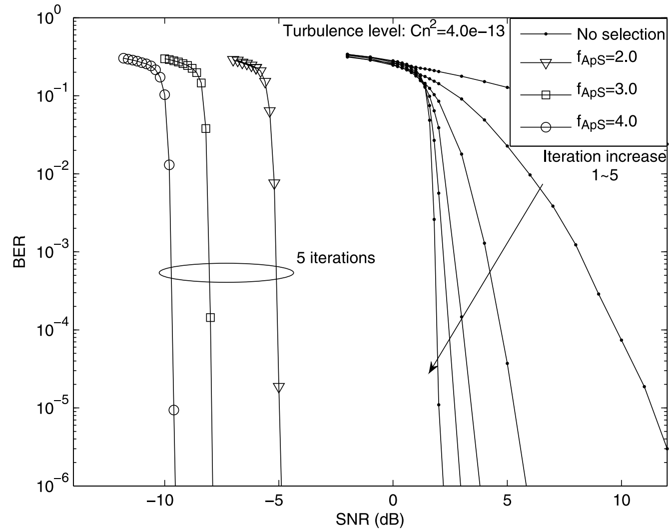

Fig. 10. BER performance comparison of the three-stage iteratively decoded G2-STBC-based ACO-OFDM MTRA systems employing the joint ApS scheme having ApS factors of 2, 3, and 4, respectively, as well as operating without ApS, communicating over the strongly turbulent channel.

is much more significant under the strongly turbulent channel of $C_n^2 = 4 \times 10^{-13}$, particularly for a large ApS factor of 4.

2) BER Performance: Fig. 9 compares the BER performance of the three-stage iteratively decoded G2-STBC-based ACO-OFDM MTRA system relying on the proposed joint ApS scheme having the ApS factors of 2, 3, and 4, respectively, to that of its counterpart operating without ApS, when communicating over the weakly turbulent channel of $C_n^2 = 4 \times 10^{-15}$. For the system operating without ApS, the BER convergence of the three-stage iterative decoder is portrayed in Fig. 9, where it can be seen that the system is capable of converging to a vanishing low BER, with the "turbo-cliff" of the BER curve occurring approximately at $\text{SNR} = 2.1$ dB after $I_{\text{outer}} = 5$ iterations. For the proposed system assisted by our joint ApS scheme having the ApS factors of 2, 3, and 4, by contrast, the turbo-cliff of the BER curve occurs at the SNR values of 0.9, 0.3, and 0.0 dB, respectively.

Similarly, Fig. 10 compares the BER performance of the two systems assisted by the joint ApS scheme as well as operating without ApS, when communicating over the strongly turbulent channel of $C_n^2 = 4 \times 10^{-13}$. It is shown in Fig. 10 that for the ApS-assisted system having an ApS factor of 2, a vanishing low BER is achieved at $\text{SNR} = -5$ dB, which matches the prediction by the EXIT chart analysis presented in Fig. 7. When the ApS factor is increased to 3 and 4, a further performance enhancement is attained, and the turbo-cliff of the system's BER curve occurs at the SNR values of -8 and -9.7 dB, respectively. By contrast, the system operating without ApS can only attain a vanishing low BER at approximately $\text{SNR} = 2$ dB. By comparing Figs. 9 and 10, it can be confirmed again that the performance enhancement achievable by ApS is much more significant under strongly turbulent channel conditions. Specifically, given the ApS factor of 4, the turbo-cliff of the BER curve occurs at approximately $\text{SNR} = -9.7$ dB under the strongly turbulent level of $C_n^2 = 4 \times 10^{-13}$, whereas it requires $\text{SNR} = 0$ dB to attain a vanishingly low BER under the weakly turbulent channel of $C_n^2 = 4 \times 10^{-15}$.

V. Conclusion

In this paper, we have conceived a joint ApS scheme for a three-stage iteratively decoded ACO-OFDM-based MTRA system operating in the FSO turbulence channel. Our main contribution has been the demonstration that such ApS scheme is capable of substantially improving the system's achievable diversity gain, BER performance, and throughput, while imposing moderate hardware complexity. Thus, the ApS scheme could enhance the link reliability in vehicle-to-infrastructure and vehicle-to-vehicle communications. Moreover, our results have demonstrated that the performance gain obtained by the novel joint ApS-assisted MTRA OW system is more significant under strongly turbulent channel conditions.

References

[1] V. W. S. Chan, "Free-space optical communications," *IEEE J. Lightw. Tech.*, vol. 24, no. 12, pp. 4750–4762, Dec. 2006.

[2] D. K. Borah and D. G. Voelz, "Pointing error effects on free-space optical communication links in the presence of atmospheric turbulence," *IEEE J. Lightw. Tech.*, vol. 27, no. 18, pp. 3965–3973, Sep. 2009.

[3] P. Marcsh and G. P. Fettweis, *Coordinated Multi-Point in Mobile Communications: From Theory to Practice*. New York, NY, USA: Cambridge Univ. Press, 2011.

[4] J. Zhang, R. Zhang, G. Liu, and L. Hanzo, "Remote coalition network for base station cooperation aided multicell processing," *IEEE Trans. Veh. Technol.*, vol. 61, no. 3, pp. 1406–1415, Mar. 2012.

[5] A. Jahn *et al.*, "Evolution of aeronautical communications for personal multimedia services," *IEEE Commun. Mag.*, vol. 41, no. 7, pp. 36–43, Jul. 2003.

[6] Q. Vey, A. Pirovano, J. Radzik, and F. Garcia, "Aeronautical Ad hoc network for civil aviation," in *Communication Technologies for Vehicles*, Cham, Switzerland: Springer, 2014, pp. 81–93.

[7] D. Medina, F. Hoffmann, F. Rossetto, and C.-H. Rokitansky, "Routing in the airborne Internet," in *Proc. ICNS*, Herndon, VA, USA, May 11–13, 2010 pp. A7-1–A7-10.

[8] D. Medina, *Geographic Load Share Routing in the AIRBORNE INTERNET*. Munchen, Germany: Herbert Utz Verlag, 2011.

[9] E. Haas, "Aeronautical channel modeling," *IEEE Trans. Veh. Technol.*, vol. 51, no. 2, pp. 254–264, Mar. 2002.
[10] J. Haque, "An OFDM Based Aeronautical Communication System," Ph.D. dissertation, Univ. South Florida, Tampa, FL, USA, 2011.
[11] J. Kuchar and A. C. Drumm, "The traffic alert and collision avoidance system," *Lincoln Lab. J.*, vol. 16, no. 2, pp. 277–296, 2007.
[12] E. Williams, "Airborne collision avoidance system," in *Proc. SCS*, vol. 47, pp. 97–110, 2004.
[13] "Airborne Seperation Assurance Systems (ASAS)," EUROCONTROL, Brussels, Belgium. [Online] Available: http://www.skybrary.aero/index.php/Airborne_Separation_Assurance_Systems_(ASAS)
[14] S. Bretmersky, V. K. Konangi, and R. J. Kerczewski, "Comparison of VDL modes in the aeronautical telecommunications network," in *Proc. IEEE Aerosp. Conf.*, 2002, vol. 3, pp. 3-1183–3-1190.
[15] S. Nicol, G. Wlton, L. Westbrook, and D. Wynn, "Future satellite communication to military aircraft," *J. Electron. Commun. Eng.*, vol. 12, no. 1, pp. 15–26, Feb. 2000.
[16] G. Berzins, R. Phillips, J. Singh, and P. Wood, "Inmarsat-worldwide mobile satellite services on seas, in air and on land," in *Malaga Int. Astron. Fed. Congr.*, 1989, vol. 1.
[17] E. J. Lee and V. W. S. Chan, "Part 1: Optical communication over the clear turbulent atmospheric channel using diversity," *IEEE J. Sel. Areas. Commun.*, vol. 22, no. 9, pp. 1896–1906, Nov. 2004.
[18] J. Armstrong and A. J. Lowery, "Power efficient optical OFDM," *Electron. Lett.*, vol. 42, no. 6, pp. 370–372, Mar. 2006.
[19] W. Xu, M. Wu, H. Zhang, X. You, and C. Zhao, "ACO-OFDM specified recoverable upper-clipping with efficient detection for optical wireless communications," *IEEE Photon. J.*, vol. 6, no. 5, Oct. 2014, Art. ID. 7902617.
[20] B. Ranjha and M. Kavehrad, "Hybrid asymmetrically clipped OFDM based IM/DD optical wireless system," *IEEE J. Opt. Commun. Netw.*, vol. 6, no. 4, pp. 387–396, Apr. 2014.
[21] N. Fernando, H. Yi, and E. Viterbo, "Flip-OFDM for unipolar communication systems," *IEEE Trans. Commun.*, vol. 60, no. 12, pp. 3726–3733, Dec. 2012.
[22] I. B. Djordjevic, B. Vasic, and M. A. Neifeld, "LDPC-coded OFDM for optical communication systems with direct detection," *IEEE J. Sel. Topics Quantum, Electron.*, vol. 13, no. 5, pp. 1446–1454, Sep./Oct. 2007.
[23] I. B. Djordjevic and H. G. Batshon, "LDPC-coded OFDM for heterogeneous access optical networks," *IEEE Photon. J.*, vol. 2, no. 4, pp. 611–619, Aug. 2010.
[24] C. Chen, W. D. Zhong, X. Li, and D. Wu, "MDPSK-based nonequalization OFDM for coherent free-space optical communication," *IEEE Photon. Technol. Lett.*, vol. 26, no. 16, pp. 1617–1620, Aug. 2014.
[25] S. Sanayei and A. Norsratinia, "Antenna selection in MIMO systems," *IEEE Commun. Mag.*, vol. 42, no. 10, pp. 68–73, Oct. 2004.
[26] T. Gucluoglu and T. M. Duman, "Performance analysis of transmit and receive antenna selection over flat fading channels," *IEEE Trans. Wireless Commun.*, vol. 7, no. 8, pp. 3056–3065, Aug. 2008.
[27] M. Gharavi-Alkhansari and A. B. Gershman, "Fast antenna subset selection in MIMO systems," *IEEE Trans. Signal Process.*, vol. 52, no. 2, pp. 339–347, Feb. 2004.
[28] A. G. Zambrana, C. C. Vázquez, B. C. Vázquez, and A. H. Gómez, "Selection transmit diversity for FSO links over strong atmospheric turbulence channels," *IEEE Photon. Technol. Lett.*, vol. 21, no. 14, pp. 1017–1019, Jul. 2009.
[29] A. Sevincer, "Transceiver Selection for Multi-Element Free-Space-Optical Communications," Ph.D. dissertation, University of Nevada, Reno, NV, USA, 2013.
[30] H. Moradi, H. H. Refai, and P. G. LoPresti, "Circular MIMO nodes with transmit selection and receive generalized selection diversity," *IEEE Trans. Veh. Technol.*, vol. 61, no. 3, pp. 1174–1181, Mar. 2012.
[31] N. D. Chatzidiamantis, D. S. Michalopoulos, E. E. Kriezis, G. K. Karagiannidis, and R. Schober, "Relay selection protocols for relay-assisted free-space optical systems," *IEEE/OSA J. Opt. Commun. Netw.*, vol. 5, no. 1, pp. 92–103, Jan. 2013.
[32] A. Goldsmith, *Wireless Communications*. New York, NY, USA: Cambridge Univ. Press, 2005.
[33] M. A. Al-Habash, L. C. Andrews, and R. L. Phillips, "Mathematical model for the irradiance probability density function of a laser beam propagating through turbulence media," *Opt. Eng.*, vol. 40, no. 8, pp. 1554–1562, Aug. 2001.
[34] J. Armstrong, "Alamouti coding for indoor optical wireless communications using ACO-OFDM," in *Proc. Conf. Rec. 43rd Asilomar Conf. Signals., Sys. Comput.*, Nov. 2009, pp. 1650–1654.
[35] M. El-Hajjar and L. Hanzo, "EXIT charts for system design and analysis," *IEEE Commun. Survey Tuts.*, vol. 16, no. 1, pp. 127–153, 1st Quart. 2014.
[36] J. Wang *et al.*, "Near-capacity three-stage MMSE turbo equalization using irregular convolutional codes," in *Proc. Int. Symp. Turbo-Coding*, Munich, Germany, Apr. 3–7, 2006, pp. 1–6.
[37] R. G. Maunder and L. Hanzo, "Iterative decoding convergence and termination of serially concatenated codes," *IEEE Trans. Veh. Technol.*, vol. 59, no. 1, pp. 216–224, Jan. 2010.
[38] A. Ashikhmin, G. Kramer, and S. ten Brink, "Extrinsic information transfer functions: Model and erasure channel properties," *IEEE Trans. Inf. Theory*, vol. 50, no. 11, pp. 2657–2673, Nov. 2004.

Junyi Jiang received the B.Eng. degree in communication engineering from Heilongjiang Institute of Science and Technology, Harbin, China, in 2009 and the M.Sc. degree (with distinction) in wireless communication from the University of Southampton, Southampton, U.K., in 2010, where he is currently working toward the Ph.D. degree with the Wireless Group.

His research interests include indoor visible light communication, free-space optical communication, and iterative detection.

Peichang Zhang received the B.Eng. degree (with first-class honors) in electronic engineering from the University of Central Lancashire, Lancashire, U.K., in 2009; the M.Sc. degree (with distinction) in wireless communications from the University of Southampton, Southampton, U.K., in 2010; and the Ph.D. degree from the Communications, Signal Processing, and Control Research Group, Department of Electronics and Computer Science, University of Southampton.

He is currently holding a lecturing position with the College of Information Engineering, Shenzhen University, Shenzhen, China. His research interests include coherent and noncoherent detection, iterative detection, and estimation.

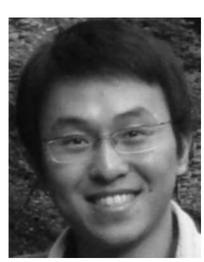

Rong Zhang (M'09) received the B.Sc. degree from Southeast University, Nanjing, China, in 2003 and the Ph.D. degree from Southampton University, Southampton, U.K., in 2009.

From January 2006 to May 2009, he was an Engineer with China Telecom and a Research Assistant with the Mobile Virtual Center of Excellence (MVCE), U.K. From August 2009 to July 2012, he was a Postdoctoral Researcher with Southampton University, after which, he took industrial consulting leave from August 2012 to January 2013 for Huawei Sweden R&D as a System Algorithms Specialist. Since February 2013, he has been appointed as a Lecturer with the Southampton Wireless Group of Electronics and Computer Science, Southampton University. He has over 40 journals in prestigious publication avenues (e.g., IEEE and OSA) and many more in major conference proceedings.

Dr. Zhan regularly serves as a Reviewer for IEEE TRANSACTIONS/journals and has been a Technical Program Committee Member/Invited Session Chair of major conferences several times. He received joint funding from the MVCE and the Engineering and Physical Sciences Research Council. He is also a Visiting Researcher under the Worldwide University Network.

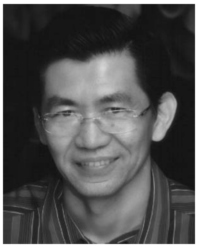

Sheng Chen (M'90–SM'97–F'08) received the B.Eng. degree in control engineering from the East China Petroleum Institute, Dongying, China, in 1982; the Ph.D. degree in control engineering from the City University London, London, U.K., in 1986; and the D.Sc. degree from the University of Southampton, Southampton, U.K., in 2005.

From 1986 to 1999, he held research and academic appointments with the University of Sheffield, Sheffield, U.K.; the University of Edinburgh, Edinburgh, U.K.; and the University of Portsmouth, Portsmouth, U.K. Since 1999, he has been with the Department of Electronics and Computer Science, University of Southampton, where he is currently a Professor of intelligent systems and signal processing. He has published over 550 research papers. His research interests include adaptive signal processing, wireless communications, modeling and identification of nonlinear systems, neural network and machine learning, intelligent control system design, evolutionary computation methods, and optimization.

Dr. Chen is a Fellow of the Institution of Engineering and Technology; a Distinguished Adjunct Professor with King Abdulaziz University, Jeddah, Saudi Arabia; and an Institute for Scientific Information Highly Cited Researcher in Engineering (March 2004). He was elected a Fellow of the United Kingdom Royal Academy of Engineering in 2014.

Lajos Hanzo (M'91–SM'92–F'04) received the M.S. degree in electronics and the Ph.D. degree from the Technical University of Budapest, Budapest, Hungary, in 1976 and 1983, respectively; the D.Sc. degree from the University of Southampton, Southampton, U.K., in 2004; and the "Doctor Honoris Causa" degree from the Technical University of Budapest in 2009.

During his 38-year career in telecommunications, he has held various research and academic posts in Hungary, Germany, and the U.K. Since 1986, he has been with the School of Electronics and Computer Science, University of Southampton, where he holds the Chair in Telecommunications. He is currently directing an academic research team, working on a range of research projects in the field of wireless multimedia communications sponsored by industry, the Engineering and Physical Sciences Research Council (EPSRC), the European Research Council's Advanced Fellow Grant, and the Royal Society's Wolfson Research Merit Award. During 2008–2012, he was a Chaired Professor with Tsinghua University, Beijing, China. He is an enthusiastic supporter of industrial and academic liaison and offers a range of industrial courses. He has successfully supervised about 100 Ph.D. students, coauthored 20 John Wiley/IEEE Press books on mobile radio communications totaling in excess of 10 000 pages, and published more than 1400 research entries on IEEE Xplore.

Dr. Hanzo is a Fellow of the Royal Academy of Engineering, the Institution of Engineering and Technology, and the European Association for Signal Processing. He is also a Governor of the IEEE Vehicular Technology Society. During 2008–2012, he was the Editor-in-Chief of IEEE Press. He has served as the Technical Program Committee Chair and the General Chair of IEEE conferences, has presented keynote lectures, and has received a number of distinctions. His published work has more than 20 000 citations. Further information on research in progress and associated publications is available at http://www-mobile.ecs.soton.ac.uk.